ACS APPLIED NANO MATERIALS

www.acsanm.org

Article

Tensile Strain-Induced Bandgap Reduction and Exciton Recombination in a Trilayer MoS_2 Nanosheet Wrinkle: Implications for Nanoscale Optoelectronic and Photonic Devices

Dario Marchiani, Nuria Jimenez-Arevalo, Ilaria Rago, Francesco Pandolfi, Gianluca Cavoto, Marco Sbroscia, Pavel Dudin, Jose Avila, Carlo Mariani, Maria Grazia Betti,* and Riccardo Frisenda*

Cite This: https://doi.org/10.1021/acsanm.5c02997

Read Online

ACCESS | Metrics & More | Article Recommendations | Supporting Information

ABSTRACT: The effects of uniaxial strain on the local band structure modification in a single wrinkle in a trilayer (3L) molybdenum disulfide (MoS_2) flake have been enlightened by combining complementary atomic force microscopy, Raman and photoluminescence microspectroscopies. Controlled wrinkles were introduced in 3L MoS_2 flakes by using buckling instability, inducing local tensile strains of up to 0.07%. The ability to induce and fabricate stable wrinkles in 3L MoS_2, which is a nanoscale system whose thickness is smaller than 2 nm, arises from the material's reduced thickness. Submicron-scale spatial mapping of the isolated wrinkle revealed a reduction of the direct bandgap by 10 meV, accompanied by a quenching of the radiative recombination of excitons in the wrinkle compatible with an antifunneling effect, where excitons drift away from lower-bandgap areas before recombination. Finally, angle-resolved photoemission microspectroscopy further demonstrated a shift of the valence band toward higher binding energies in the isolated MoS_2 wrinkle. Combining these results with the ones from optical spectroscopies results in a type-II band alignment between the flat and the strained regions, with downward shifts in both the conduction and valence bands. These new insights into the local electronic structure in locally strained 3L MoS_2 nanosheets may help the design and performance of nanoscale optoelectronic and photonic devices by enabling precise control over the excitonic properties and the energetic spatial landscape.

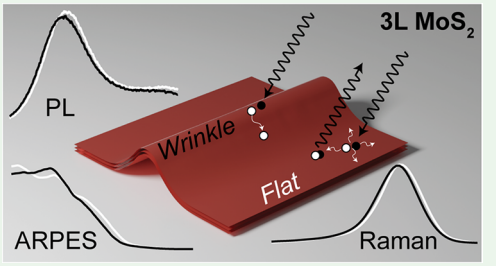

KEYWORDS: *MoS_2, local strain, Raman, photoluminescence, ARPES*

1. INTRODUCTION

Tuning the electronic structure of two-dimensional (2D) materials through mechanical deformations is a key method for tailoring their optical and electronic properties, enhancing the performance of electronic devices, and realizing novel functionality.[1−3] Among the various families of 2D materials, the remarkable mechanical flexibility of 2D transition-metal dichalcogenides (TMDs) allows these materials to withstand substantial structural curvature and to adapt to significant deformations across both in-plane and out-of-plane axes. Spatially localized strain fields, as opposed to uniform global strain, enable spatial modulation of bandgap and exciton potentials, providing a means to control the movement of neutral exciton.[4−10] This control has significant implications for applications in quantum optics, solar energy-harvesting, and light-emitting devices.[11−13]

Different strategies to induce local strain in 2D TMDs have been demonstrated in the literature, such as indentation with atomic force microscope (AFM) tips,[14,15] use of prestrained substrates,[5,16] integration of prepatterned structures,[4,17,18] and generation of bubbles.[19,20] Out-of-plane ripples at the microscopic scale are ubiquitous in 2D materials and are related to their structural stability and associated minimum-energy landscape. Controlled rippling, due to mechanical buckling, has been used previously to induce local uniaxial strain profiles in 2D materials.[4,9−11] Despite extensive research on the correlation between the mechanical strain and optical/electronic properties of TMDs, the precise mechanism underlying bandgap reduction in locally tensile-strained regions remains debated. Specifically, it is unclear whether the valence and conduction bands shift in the same direction, either both increasing or both decreasing in energy at different rates or in opposite directions, where the valence band (VB) shifts to higher energies while the conduction band shifts to lower energies. Furthermore, the strain engineering of the bandgap of TMDs could be used to efficiently manipulate excitons. In fact, if a strain gradient is created, the exciton energy is expected to vary spatially in a way similar to that of the gap itself. The first scenario, when the valence and the conduction bands move in the same direction,

Received: June 23, 2025
Revised: September 18, 2025
Accepted: September 19, 2025

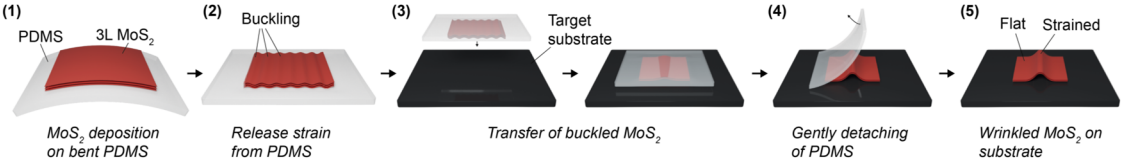

Figure 1. Fabrication scheme of wrinkled 3L MoS_2. From left to right, schematic depicting the sequential steps needed to fabricate a wrinkled MoS_2 sample on a target substrate, starting from mechanically exfoliated buckled MoS_2 on PDMS.

would result in an exciton funneling effect, where excitons migrate to the highest strain region before recombining.[4,5,21] In the second scenario, the valence band and the conduction band shift in opposite directions, leading to an antifunneling effect, causing excitons to drift away from the largest strain region.[22] Resolving this debate is essential for advancing the understanding of strain-engineered excitonic behavior in 2D materials.

In this study, an isolated wrinkle in an atomically thin trilayer (3L) MoS_2 subjected to local uniaxial strains of 0.07% has been investigated through a combination of optical and electronic spectroscopies with sub micrometer scale spatial resolution to isolate the optical/electronic response of a single homogeneous wrinkle. Local uniaxial strain is achieved by the deterministic transfer of buckled MoS_2 and controlled delamination from the substrate.[5,23] The ability to induce and fabricate stable wrinkles in 3L MoS_2, whose thickness is less than 2 nm, making it a nanoscale system, arises from the material's reduced thickness in the few-layer to monolayer regime. AFM and micro-Raman mapping allow the characterization of the single wrinkle geometry and the quantitative estimation of the strain. Spatially resolved photoluminescence (PL) mapping reveals a direct bandgap reduction of about 10 meV in the isolated wrinkle. Despite this energy shift, the overall PL emission intensity map suggests an antifunneling effect in the single wrinkle, wherein excitons drift away from the lower-bandgap strained areas before recombining, thus reducing locally the PL emission intensity. Angle-resolved photoemission spectroscopy (ARPES) micromapping unveils a rigid shift toward higher binding energies of the valence band in the uniaxial strained region as compared to the flat areas. It is worth noting that this micro-ARPES-measured valence band shift can univocally discriminate the origin of the exciton recombination in the isolated homogeneous wrinkle, finally settling the controversial open question. In fact, combining the VB energy shift with the bandgap reduction observed in PL, an antifunneling effect is clearly established, arising from a type-II band alignment in the flat-strained interface of 3L MoS_2. In this scenario, the conduction band experiences a larger shift than the valence band, leading to an exciton migration away from the strained regions. The understanding of the effects of local strain in an isolated homogeneous wrinkle in a 2D material, thanks to micro-spectroscopical analysis, can pave the way for a finer control of excitonic motion with potential applications in photovoltaics, quantum optics, and 2D optoelectronic devices. Overall, new insights into strain-induced effects in few-layer MoS_2 can significantly advance applied nanoscience by enabling precise spatial control of electronic and excitonic properties at the nanoscale.[24] The strain control over exciton dynamics and band structure modulation can open new pathways for designing high-performance nanoscale optoelectronic and quantum devices, flexible sensors, and energy-harvesting systems. Our findings, which extend our understanding of local strain from monolayers to few-layers, where interlayer coupling and stacking can have important effects in device performance under strain, contribute to nanoscale optoelectronic and photonic devices based on thin van der Waals materials, promoting the development of layered strained structures with spatially tunable functionalities for advanced nanotechnologies and flexible electronics applications.

2. EXPERIMENTAL SECTION

2.1. Sample Fabrication. Starting from a bulk MoS_2 crystal (Moly Hill mine, Quebec, Canada), atomically thin flakes are deposited onto an elastomeric substrate (Gel-Film WF X4 6.0, GelPak), which is prestretched by ≈20% of tensile uniaxial strain (step 1, Figure 1). The prestretching is achieved by mounting the elastomeric substrate in a three-point bending setup. Subsequently, after the deposition of flakes, releasing the tension in the elastomeric substrate produces well-aligned wrinkles in the MoS_2 layers perpendicular to the initial uniaxial strain axis in the substrate (step 2, Figure 1); see also Figure S1. Thanks to a deterministic transfer method (steps 3 and 4, Figure 1), we have deposited the buckled MoS_2 flake onto a SiO_2/Si substrate (sample 1 used in μ-Raman and μ-PL measurements; see Figure 1 for AFM characterization of this sample), partially covering a predeposited Au pad directly connected to the conductive highly doped Si substrate, or onto a graphene/SiC substrate (sample 2 used in μ-ARPES measurements; see Figure S10 for an AFM characterization of this sample). The transfer method allows one to reliably produce wrinkled MoS_2 samples on a target substrate (step 5, Figure 1).

2.2. AFM Measurements. Topographic measurements were performed in air with a Park Systems NX10 AFM (Suwon, Republic of Korea) in tapping mode by using a Nanosensors PPP-NCHR AFM tip (Neuchatel, Switzerland) by collecting micrographs of 1024 × 1024 pixels at a cantilever scanning rate of 0.1 Hz (speed ≈ 5 μm/s).

2.3. μ-Raman Measurements. The μ-Raman experiments were performed in UHV in a backscattering configuration by using as excitation a Nd:YVO4 laser at 532.2 nm. The laser and the signal were sent through a UHV-compatible NA = 0.82, 60× objective (IT-APO532-RAMAN082, Attocube) focused on the sample in a 0.5 μm spot size with a total power of 100 μW to avoid sample damage. A spectrograph and scanning monochromator (SpectraPro HRS-500, Princeton Instruments) equipped with a 1200 grooves/mm grating was employed to analyze the signal, which was detected by a back-illuminated liquid N_2-cooled Si CCD camera. The UHV-compatible Raman sample holder was mounted onto a hexapode piezoelectric stage that can be moved with steps as small as 50 nm. The data were then analyzed using custom routines written in MATLAB (Mathworks).

2.4. μ-Photoluminescence Measurements. The μ-PL measurements were performed in the same way as the μ-Raman experiments, with the only difference being the monochromator equipped with a 300 grooves/mm grating to record a larger portion of the spectrum in one shot.

2.5. μ-ARPES Measurements. The μ-ARPES experiment was conducted at the ANTARES beamline of the SOLEIL Synchrotron (Saint-Aubin, France). The excitation was given by linearly horizontally polarized photons of 95 eV (flux on the sample ≈ 10^{10} photons/s), and the emitted photoelectrons were analyzed in energy and angle by a hemispherical electron analyzer with a vertically confining entrance slit, which enabled accurate mapping of electronic states by restricting the angular acceptance in one direction, improving momentum resolution for band structure studies. Beam focusing was achieved using Fresnel zone plates, ensuring spatial selectivity better than 0.5 μm (see also Figure S9). This is essential for probing inhomogeneous materials and

https://doi.org/10.1021/acsanm.5c02997
ACS Appl. Nano Mater. XXXX, XXX, XXX−XXX

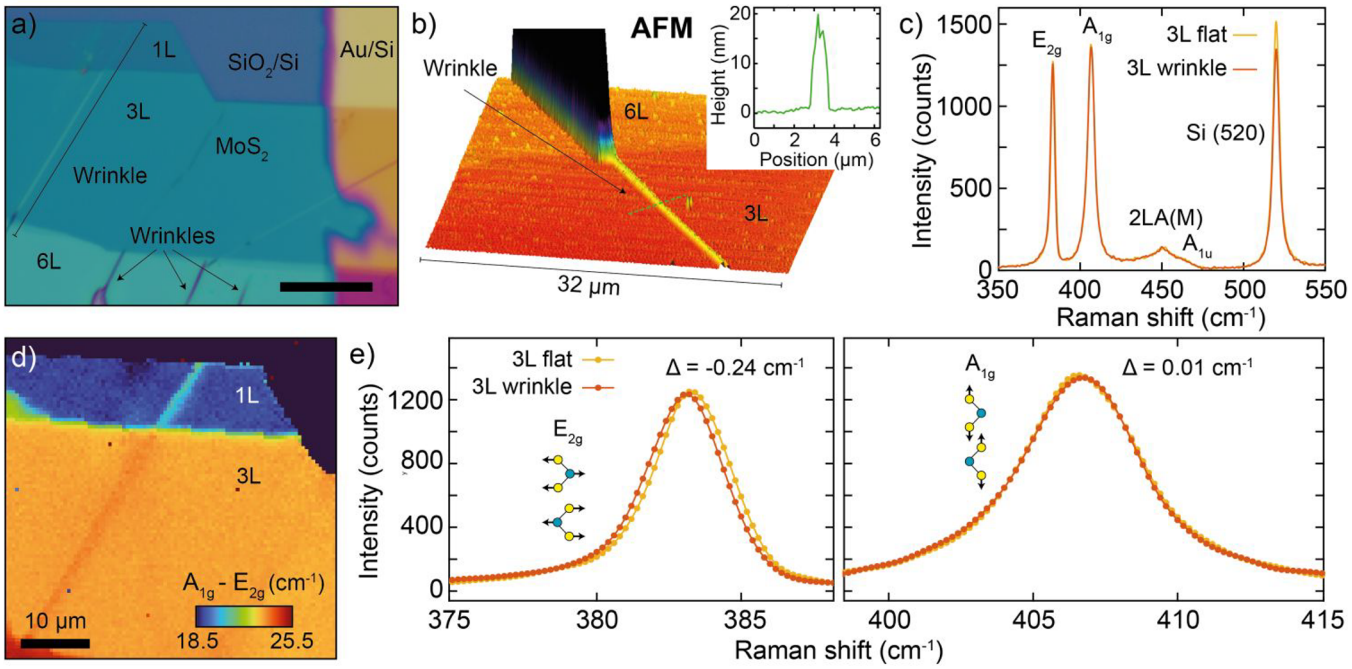

Figure 2. Local uniaxial strain profile characterization in wrinkled 3L MoS_2. (a) Optical microscope photograph of MoS_2 transferred onto SiO_2/Si and Au/Si. (b) Atomic force microscopy of the 3L and 6L region of the sample. Inset: Line profile taken along the wrinkle. (c) Representative Raman spectra of 3L MoS_2 recorded on the flat region (orange) and on the wrinkle (red). (d) Map of the difference between the A_{1g} and E_{2g} peak positions extracted from Lorentzian peak fitting. (e) High-resolution Raman spectra in the region of the E_{2g} (left) and A_{1g} (right) peaks recorded in the flat (orange) and in the strained (red) 3L MoS_2.

nanoscale regions within 2D samples. During the measurements, the sample was kept at a low temperature (70 K) to reduce beam damage during ARPES measurements (typically lasting ≈30−60 min).

3. RESULTS AND DISCUSSION

3.1. Quantitative Strain Analysis via AFM and μ-Raman Mapping. The fabrication of a localized uniaxial strain profile in 3L MoS_2 exploits the buckling instability in mechanically exfoliated flakes that leads to the formation of wrinkles by buckling-induced delamination (see Methods in Section 2.2 and Figure 1).[25,26] As reported in previous works,[27] this fabrication method generates periodic wrinkles whose periodicity is dependent on the thickness of the MoS_2 flakes. Figure 2a shows an optical microscopy image of the as-fabricated sample, where regions with different numbers of layers (1L, 3L, and 6L) can be identified in the MoS_2 flake. It is worth noting that the MoS_2 flake is flat, while the buckled regions collapsed into a few wrinkles, which are visible in the optical image.

To confirm that the local features observed in the optical image are indeed due to wrinkles, we performed topographic measurements. The topography of the flake from AFM mapping is reported in Figure 2b. In the 3L MoS_2 flake, the delaminated wrinkle is visible, and a line profile for determining its geometry is shown in the inset of the figure. The maximum in-plane uniaxial tensile strain ε (along the axis perpendicular to the wrinkle) accumulated on top of the wrinkle can be estimated according to the relation:

$$\varepsilon = \frac{\pi^2 h \delta}{(1-\sigma^2)\lambda^2}$$

where σ is the MoS_2 Poisson's ratio (σ = 0.27),[14,28] h is the thickness of the flake, and δ and λ are the height and width of the wrinkle, respectively.[5,29] The values for δ and λ are extracted from the AFM topography of the isolated wrinkle ($\delta = (18 \pm 2)$ nm and $\lambda = (800 \pm 100)$ nm). For the thickness h, we use the value of h = 1.95 nm for a 3L MoS_2, as deduced by quantitative optical transmission microscopy, Raman spectroscopy, and photoluminescence. Thus, the estimated uniaxial strain is (0.06 ± 0.02)%. for the isolated wrinkle in the 3L MoS_2 flake.

After the topographic characterization of the wrinkle isolated in the flat region of a 3L MoS_2 flake, μ-Raman mapping using a 532 nm laser (see Section 2.3) can unravel the different optical response of the flat and buckled regions. The Raman spectra taken on the flat and wrinkled 3L MoS_2, reported in Figure 2c, show the typical E_{2g} and A_{1g} bands at about 383 and 407 cm^{-1}, respectively, and the broader 2LA(M) and A_{1u} structures at about 450 cm^{-1}.[30−32] The peak at 520 cm^{-1} is due to the Si substrate, and its intensity variation between the flat and strained MoS_2 regions is consistent with the change in the optical contrast of strained MoS_2, visible in the optical photograph of Figure 2a. To assess the homogeneity of the flat and strained MoS_2 sample, a spatial micro-Raman mapping was conducted by performing a raster-scanning of the sample in steps of 500 nm over an area of 50 × 50 μm^2 and acquiring a Raman spectrum at each position. Figure 2d shows the difference between the A_{1g} and E_{2g} peak positions, which is a parameter known to depend on the MoS_2 thickness and on the changes in strain or doping.[31,33,34] All of the different regions already discussed in the optical photograph of Figure 2a can be clearly identified, with the spatial features of the map showing that the terraces are homogeneously flat and that the wrinkle is also homogeneous along its length. See also Figure S2 for histograms of the A_{1g} and E_{2g} Raman shifts. It is worth noting that the $A_{1g}-E_{2g}$ wavenumber difference increases when going from 1L MoS_2 to 6L MoS_2, as expected from the literature.[33] Thus, the observed increase in the $A_{1g}-E_{2g}$ Raman shift difference in the 3L isolated wrinkle as compared to the 3L flat region cannot be

https://doi.org/10.1021/acsanm.5c02997
ACS Appl. Nano Mater. XXXX, XXX, XXX−XXX

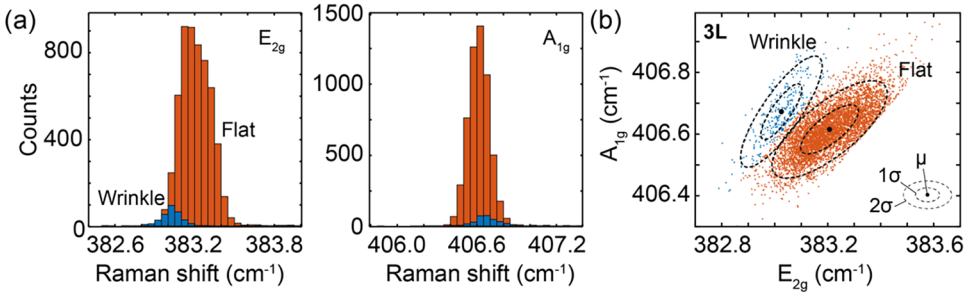

Figure 3. Local strain and charging effects from Raman analysis. (a) Histograms of the Raman shift of the E_{2g} (left) and A_{1g} (right) peak positions for 3L MoS_2 taken in the flat (red) and wrinkled (blue) regions. (b) Scatter plot of the A_{1g} peak position as a function of E_{2g} peak position in the 3L MoS_2. The red and blue points correspond to flat and wrinkle regions. Each of the two clouds of data has been fitted to a two-dimensional Gaussian peak shown by the black dot and the dashed lines, respectively, for the distribution center and the one- and two-standard-deviation boundaries.

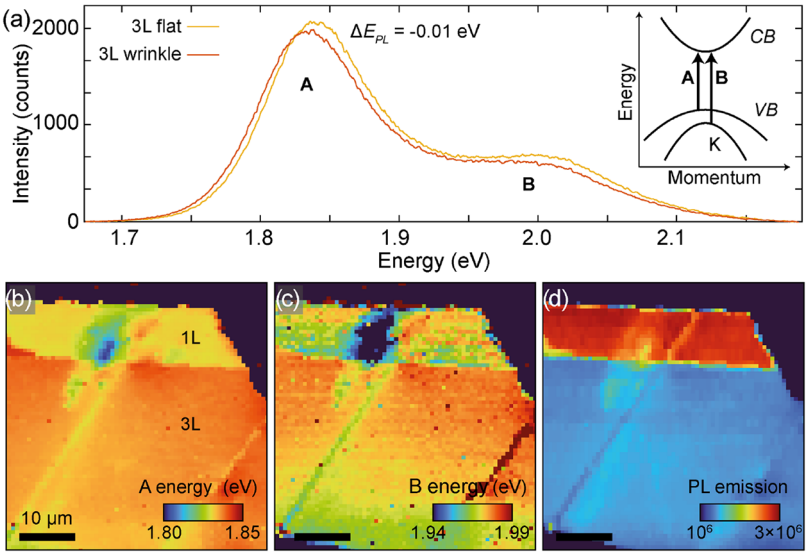

Figure 4. Photoluminescence mapping and bandgap modulation by strain. (a) Representative photoluminescence spectra of 3L MoS_2 recorded on the flat region (yellow) and on the wrinkle (red). Inset: Sketch of the band structure around the K point. (b, c) Map of the peak position of the A exciton (b) and B exciton (c). (d) Photoluminescence map of the total PL area.

caused by a delamination of the layers, which would reduce the MoS_2 interlayer coupling, thus reducing this $A_{1g}-E_{2g}$ peak difference.[35]

An accurate analysis of the μ-Raman peaks of MoS_2 can unveil the effects of the isolated wrinkle on the vibrational spectrum. Figure 2e reports high-resolution μ-Raman spectra of the E_{2g} and A_{1g} bands in flat (yellow curve) and wrinkled MoS_2 (red curve) regions. The E_{2g} vibrational band shows a red-shift of $\Delta\omega_{E_{2g}} = -0.24\ cm^{-1}$ in the wrinkled MoS_2, as compared to the flat one. On the other hand, the out-of-plane mode A_{1g} vibrational bands in flat and wrinkled regions are almost indistinguishable, with a very tiny Raman shift ($\Delta\omega_{A_{1g}} = 0.01\ cm^{-1}$). The MoS_2 Raman band energy positions can be affected by strain ε and by charging n according to the equation:

$$\Delta\omega = \frac{\partial\omega}{\partial\varepsilon}\Delta\varepsilon + \frac{\partial\omega}{\partial n}\Delta n$$

where $\frac{\partial\omega}{\partial\varepsilon}$ and $\frac{\partial\omega}{\partial n}$ are the Raman peak gauge factors for strain and charging. Local charging effects in the isolated wrinkle are negligible, considering the values of $\frac{\partial\omega}{\partial n}$ for the A_{1g} and E_{2g} 1L MoS_2 bands reported in the literature.[36,37] Furthermore, it is well-known that the E_{2g} peak position is mainly influenced by in-plane strain. Using $\frac{\partial\omega}{\partial\varepsilon}$ of a MoS_2 trilayer from the literature,[38] the strain on the wrinkle results in $\varepsilon_{Raman} = (0.08 \pm 0.01)\%$, perfectly in agreement with the strain estimated from the AFM image $\varepsilon_{AFM} = (0.06 \pm 0.02)\%$. In the rest of the article, we will use the average value between ε_{Raman} and ε_{AFM} for the uniaxial strain, that is, $(0.07 \pm 0.01)\%$.

A statistical analysis of the Raman peak positions is shown in Figure 3. The histograms of the E_{2g} and A_{1g} peak positions built from the 3L flat and wrinkle Raman spectra are reported in Figure 3a. The division of the spectra in flat and wrinkle regions is done automatically using the $A_{1g}-E_{2g}$ Raman shift difference to discriminate between the two regions, as shown in Figure S3. The histograms have a Gaussian shape with small dispersions, and in the case of the E_{2g} histogram, the separation between flat and wrinkle regions is evident. The shift observed for the E_{2g} peak, which is negligible for the A_{1g} peak, is consistent with the previous analysis made on single high-resolution spectra. The E_{2g} and A_{1g} Raman shifts are correlated by strain and charging effects, as discussed previously; such a correlation can be visualized by a scatter plot of these two variables as commonly done in the literature.[36,37,39]

In Figure 3b, the position of the E_{2g} versus the A_{1g} peak, extracted from all of the Raman spectra of the trilayer and color-

https://doi.org/10.1021/acsanm.5c02997
ACS Appl. Nano Mater. XXXX, XXX, XXX−XXX

coded for the flat and wrinkled regions, is shown. Here, the data for flat and wrinkled regions are distributed in two data clouds, which can be clearly distinguished. Each of these data clouds has been fitted to a two-dimensional Gaussian distribution whose center and one- and two-standard-deviation contours are shown in the figure. The flat region distribution has a center located at $(E_{2g}, A_{1g}) = (383.22, 406.62)\ cm^{-1}$, while the wrinkled region is located at $(E_{2g}, A_{1g}) = (383.03, 406.67)\ cm^{-1}$, confirming the previous analysis performed on single high-resolution spectra. As discussed previously, strain and charge doping can be expressed linearly in terms of the Raman shifts (E_{2g}, A_{1g}) since, at low levels of these two quantities, their effects are decoupled from each other. In Figure S3, we plot the isostrain and isocharge concentration axes. From the scatter plot, it is evident that the wrinkle affects primarily the strain of 3L MoS_2, resulting in a tensile uniaxial strain of approximately 0.075%, and has a small effect also on the charge concentration. Using $\frac{\partial\omega}{\partial n}$ values from literature for 1L MoS_2 (normalized to take into account the 3L thickness),[40] we find, as an upper estimate, the wrinkle-induced electron doping of $-0.1 \times 10^{12}/cm^2$, a negligible change in doping that reflects strain and substrate interaction effects.

3.2. Photoluminescence Response to Local Tensile Strain. The effects of local strain in the wrinkled region can significantly influence the photoluminescence signal. To investigate how localized tensile strain in the isolated wrinkle affects the optical response, spatially resolved μ-PL mappings of the 3L MoS_2 sample in both the flat and wrinkled regions are shown in Figure 4a. While 3L MoS_2 is an indirect bandgap semiconductor, its PL spectrum is primarily dominated by direct-gap transitions at the K point of the Brillouin zone, occurring between the conduction and valence bands, the latter of which is split due to interlayer interactions and spin−orbit coupling.[41,42] The direct-gap transitions appear as two resonances in the PL spectra, associated with two excitons: the A exciton at lower energy and a higher-energy shoulder corresponding to the B exciton (see the inset of Figure 4a). Comparing the spectra, in the one acquired on top of the wrinkle, both the A and B excitons are shifted to lower energies with respect to the spectrum measured on the flat region, with an overall shift of the excitonic resonances $\Delta E_{PL} = -10$ meV. The observed energy shift aligns with previous reports on local strain effects in wrinkled few-layer MoS_2.[5,21,43]

In Figure 4b,c the positions of the peaks corresponding to A and B excitons are shown, respectively, as obtained by raster-scanning the sample in 500 nm steps over a $50 \times 50\ \mu m^2$ area and fitting the individual PL spectra with Lorentzian peaks (see Figure S4 for some examples of multipeak fit of the 3L MoS_2 PL spectra). The shifts of both A and B excitons are homogeneous along the wrinkle length, and they are both downshifted in energy, clearly indicating a bandgap reduction. These energy shifts can also be seen in the histogram representations reported in Figure S5. Interestingly, apart from the energy shift of the exciton PL emission (and the total PL intensity as discussed in the following paragraph), we do not observe additional line shape changes between the flat and the strained regions, indicating that the strain effects on the trion population is negligible in our case, possibly because the strain levels probed are very small (see also Figure S6).[44,45] The spectral weight of trions in our mechanically exfoliated 3L MoS_2 is also low compared to thinner regions, e.g., the 1L region (Figure S7), or compared to chemically vapor deposition (CVD)-grown MoS_2.[46−48] The small trion population suggests a low intrinsic doping level in our sample, which is typically related to a low defect density.

Besides the energy shift, the PL intensity in the wrinkled region is notably lower than that in flat 3L MoS_2. This intensity reduction is evident in the μ-PL total emission intensity mapping shown in Figure 4d and from the histogram shown in Figure S8. The reduction of PL emission from uniaxially strained regions has been previously reported by Conley et al.,[49] where a strong PL reduction in monolayer (1L) MoS_2 on SU8 photoresist deposited on polycarbonate has been observed, whereas bilayer (2L) MoS_2 remained largely unaffected. Similarly, Li et al. reported a decrease in PL intensity with increasing uniaxial strain in 1L MoS_2 on poly(vinyl alcohol).[50] Both studies attributed this effect to a strain-induced direct-to-indirect bandgap transition in monolayer MoS_2. Other articles that report a PL intensity reduction in MoS_2 due to tensile strain, but do not comment on the physical origin, are from Christopher et al. and Çakıroğlu and coauthors.[51,52] Castellanos-Gomez et al. in ref 5 studied the PL of wrinkle MoS_2 on an elastomeric substrate (Gel-Fim WF × 4 6.0 mil). The authors did not explicitly comment on the strain effects for the PL intensity, but focused on the discussion on the shift of the exciton peak. Nevertheless, a PL spectrum of a 3L MoS_2 in the Supporting Information of that article shows a moderate intensity quenching on a wrinkle without a clear change in line shape, more similar to our case. In general, strain-related quenching of the PL is much less prominent in few-layer cases than in the monolayer case.[46,53] On the other hand, multilayer flakes can have larger PL quenching, which typically do not depend only on the strain but on the geometry of the wrinkle, as shown for example in ref[43] by Deng and coauthors. Overall, our moderate PL intensity quenching is compatible with the results from the literature. Finally we notice that also the fabrication method (e.g., CVD versus mechanical exfoliation) or the biaxial/uniaxial nature of strain can influence the strain-induced PL quenching.[53−56]

Photoluminescence and Raman measurements carried out here on a single isolated one-dimensional wrinkle of a 3L MoS_2 flake confirm the spectral dependence observed in strained TMDs with respect to flat crystals. However, in order to get the complete energetic landscape in this locally uniaxially strained MoS_2, angle-resolved photoemission spectroscopy micromapping can discriminate the effect of local tensile strain on the band structure and enlighten the very origin of the PL intensity reduction observed in locally strained regions. ARPES measurements spatially resolved at the micron scale are still experimentally unavailable on an isolated wrinkle, and whether the valence and conduction bands shift in the same or in opposite directions is still an open question.

3.3. Band Structure Modification Revealed by μ-ARPES Micromapping. μ-ARPES measurements have been performed at the ANTARES beamline at SOLEIL, comparing the band structure of flat and strained 3L MoS_2.[57] To perform this experiment, we used a second sample, still consisting of wrinkled 3L MoS_2, but deposited on a different substrate, namely, Gr/SiC. The sample fabrication was identical to the one used for the optical spectroscopies measurements, and the wrinkle geometry and strain level were also comparable (see Figure S10), This change of the substrate in μ-ARPES measurements was dictated by the requirements of a conductive and ultraflat substrate to measure bands by ARPES. In this case, the Gr/SiC substrate is an excellent one as it provides high electrical conductivity and ultraflat topography. Unfortunately, the high electrical con-

https://doi.org/10.1021/acsanm.5c02997
ACS Appl. Nano Mater. XXXX, XXX, XXX−XXX

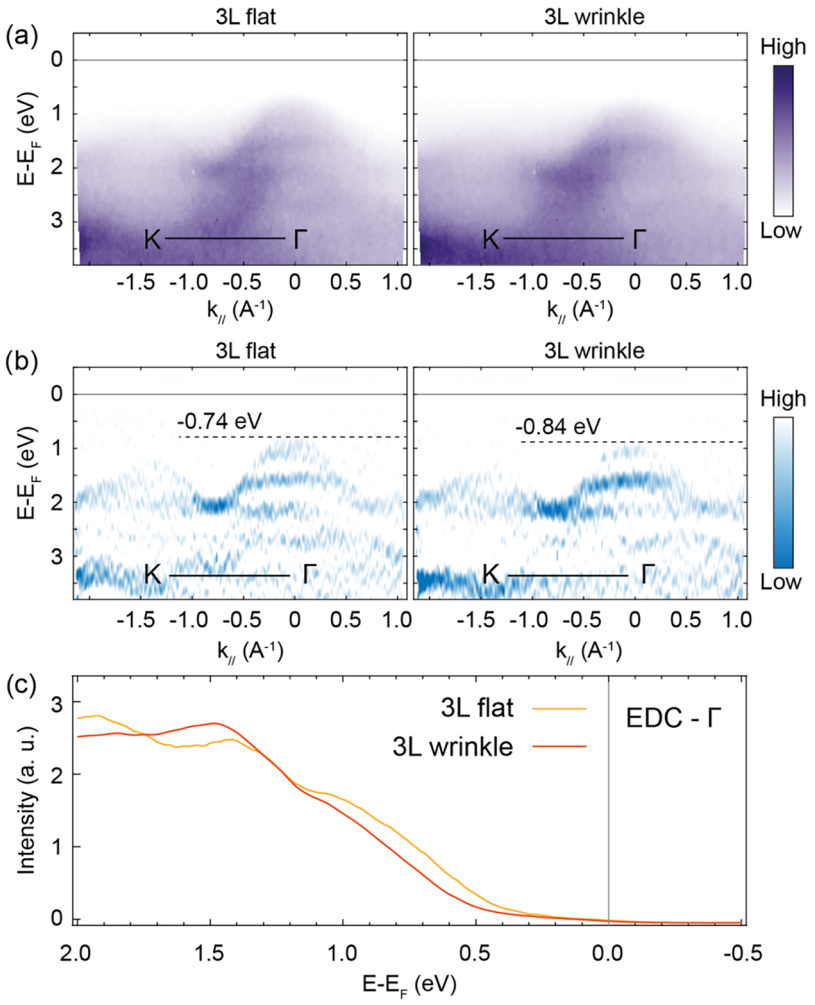

Figure 5. Valence band shift in locally uniaxially strained 3L MoS_2. (a) μ-ARPES images acquired on flat (left) and wrinkled (right) 3L MoS_2 along the Γ−K direction and taken at a photon energy of 95 eV. (b) Curvature spectra of the (a) panel. (c) Energy dispersive curve (EDC) at Γ taken from the measurements in the (a) panel.

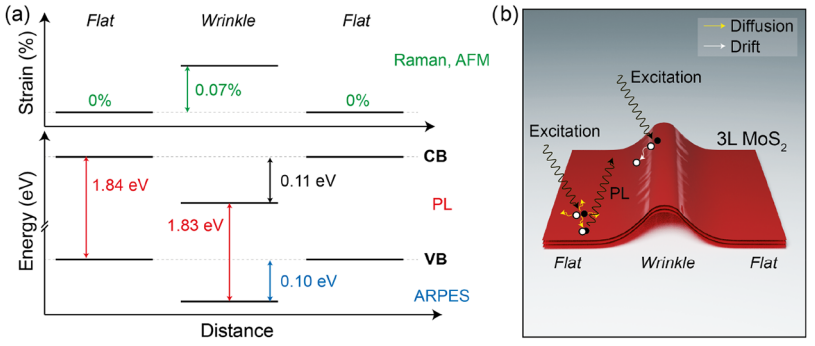

Figure 6. Energetic landscape in locally uniaxially strained 3L MoS_2. (a) Schematic profile of strain (top) and band structure (bottom curves represent the maximum of the valence band VB and the minimum of the conduction band CB) of 3L MoS_2 versus distance under nonuniform strain in our experiment. The values for the strain, bandgap, and VB are extracted, respectively, from spatially resolved Raman/AFM, PL, and μ-ARPES experiments. (b) Nonuniform strain profile generated by the wrinkle in 3L MoS_2 favors the drift of holes away from the wrinkle, reducing the radiative recombination of excitons.

ductivity has consequences on the PL emission, which is highly quenched, and on the degradation of optical contrast of 3L MoS_2, preventing high-resolution optical spectroscopy measurements.

The angular resolved photoemission intensity maps, taken along the Γ-K direction, acquired at 95 eV photon energy for the 3L MoS_2/Gr/SiC substrate are reported in Figure 5a, measured in the flat region and in the isolated wrinkle (respectively, left and right panels), and the corresponding energy distribution curves integrated about 0.4 Å^{-1} around the Γ point are reported in Figure 5c. Figure 5b reports the 2D curvature calculated from the ARPES spectra. As expected for 3L MoS_2, the valence band

https://doi.org/10.1021/acsanm.5c02997
ACS Appl. Nano Mater. XXXX, XXX, XXX−XXX

maximum (VBM) is located at the Γ point of the Brillouin zone, with a secondary local maximum at K, which is the location of the initial state for the PL emission discussed earlier. A comparison between the band structures of the flat and wrinkled regions reveals no significant topological modifications, indicating that the wrinkle does not disrupt the interlayer coupling, consistent with the Raman measurements reported in Figure 1. The primary effect of the strain is a downshift (≈100 meV) of the VBM in the wrinkled region and a slight increase in the density of states at about 1.4 eV binding energy (∼1 eV below the VBM). These observations, albeit obtained on a 3L system, are in agreement with density functional theory (DFT) calculations on a single-layer MoS_2, which predict an energy gap reduction[58] and an increase of the Mo-derived partial density of states at about 1 eV below the VBM[59] under tensile strain. While both 1L and 3L MoS_2 experience a reduction of the bandgap under tensile strain, the magnitude and details of the response depend on the number of layers.

The spatially resolved ARPES measurements complemented by the PL results allow us to univocally determine the energetic band diagram in this isolated wrinkle with respect to the flat region, as sketched in Figure 6a. The 0.07% tensile strain in the single wrinkle causes the reduction of the bandgap, with a downward differential energy shift of the VBM (−0.10 eV) and CBM (−0.11 eV). This modification of the electronic structure (type-II alignment between the valence and conduction bands) can then lead to the antifunneling of excitons or to a destabilization of excitons since the energy minimum for electrons and holes is located at different positions in space (when the electron−hole pair is generated in close proximity to the wrinkle) as sketched in Figure 6b where exciton diffusion in flat MoS_2 versus type-II-induced drift in the wrinkle is shown. This process can explain the local quenching of the PL emission observed in the wrinkle. The antifunneling effect observed here, where excitons drift away from the maximally strained regions, different from the behavior commonly observed in 1L MoS_2, shows that layer-dependent response to strain is not a simple extension of the monolayer physics. Focusing on 3L MoS_2 extends strain engineering beyond the 1L case and provides new insights into the interplay between strain and optoelectronic properties in thicker than 1L cases.

4. CONCLUSIONS

A uniaxial and homogeneous wrinkle produced exploiting the buckling instability in a 3L MoS_2 flake constitutes a paradigmatic playground to correlate optical and electronic responses in strained 2D materials. 3L MoS_2, whose thickness is less than 2 nm, and its wrinkles, whose out-of-plane size is typically in the tens of nanometers range, are both nanoscale objects. The lattice expansion in the isolated wrinkle of 0.07% as determined by atomic force microscopy and μ-Raman mapping induces a direct bandgap reduction of 10 meV, as detected by PL. The energetic landscape, as deduced by PL and angular resolved photoemission, univocally enlightens an antifunneling effect, where the excitons move away from the strained wire before undergoing radiative recombination. Furthermore, a slightly different shift toward higher binding energies of both valence and conduction bands in the isolated wrinkle univocally discriminates the origin of the exciton recombination. The combination of complementary electron and optical microspectroscopies unravels the effects of local strain in this exemplary isolated wrinkle in a 2D material, constituting a reference in the control of the excitonic motion in 2D materials. Such a control can have important implications for optoelectronic and photonic devices based on locally strained semiconducting nanosheets, such as few-layer MoS_2.

■ ASSOCIATED CONTENT

Supporting Information

The Supporting Information is available free of charge at https://pubs.acs.org/doi/10.1021/acsanm.5c02997.

Sample fabrication, optical and atomic microscope images, statistical analysis of Raman modes, photoluminescence spectra fit, statistical analysis of excitons from photoluminescence, and micro-ARPES knife-edge measurements (PDF)

■ AUTHOR INFORMATION

Corresponding Authors

Maria Grazia Betti − *Physics Department, Sapienza University of Rome, 00185 Rome, Italy;* orcid.org/0000-0002-6244-0306; Email: mariagrazia.betti@uniroma1.it

Riccardo Frisenda − *Physics Department, Sapienza University of Rome, 00185 Rome, Italy;* orcid.org/0000-0003-1728-7354; Email: riccardo.frisenda@uniroma1.it

Authors

Dario Marchiani − *Physics Department, Sapienza University of Rome, 00185 Rome, Italy;* orcid.org/0000-0003-4508-0756

Nuria Jimenez-Arevalo − *Physics Department, Sapienza University of Rome, 00185 Rome, Italy;* orcid.org/0000-0002-1945-4585

Ilaria Rago − *INFN Rome, Sapienza University of Rome, 00185 Rome, Italy*

Francesco Pandolfi − *INFN Rome, Sapienza University of Rome, 00185 Rome, Italy;* orcid.org/0000-0001-8713-3874

Gianluca Cavoto − *Physics Department and INFN Rome, Sapienza University of Rome, 00185 Rome, Italy*

Marco Sbroscia − *Physics Department, Sapienza University of Rome, 00185 Rome, Italy*

Pavel Dudin − *Synchrotron SOLEIL, Université Paris-Saclay, 91192 Gif sur Yvette, France*

Jose Avila − *Synchrotron SOLEIL, Université Paris-Saclay, 91192 Gif sur Yvette, France;* orcid.org/0000-0003-1027-5676

Carlo Mariani − *Physics Department, Sapienza University of Rome, 00185 Rome, Italy;* orcid.org/0000-0002-7979-1700

Complete contact information is available at: https://pubs.acs.org/10.1021/acsanm.5c02997

Notes

The authors declare no competing financial interest.

■ ACKNOWLEDGMENTS

This work was partially supported by the PRIN Grants TUNES (2022NXLTYN), 2D-FRONTIERS (20228879FT), and 2D-PentaSensing (P2022HT3FF), as well as by Sapienza Ateneo and Avvio alla ricerca funds, and by the Sapienza Seed of ERC 2023 FLEXSO.

https://doi.org/10.1021/acsanm.5c02997
ACS Appl. Nano Mater. XXXX, XXX, XXX−XXX

REFERENCES

(1) Miao, F.; Liang, S.-J.; Cheng, B. Straintronics with van der Waals materials. *npj Quantum Mater.* **2021**, *6* (1), 59.

(2) Qi, Y.; Sadi, M. A.; Hu, D.; Zheng, M.; Wu, Z.; Jiang, Y.; Chen, Y. P. Recent progress in strain engineering on van der Waals 2D materials: Tunable electrical, electrochemical, magnetic, and optical properties. *Adv. Mater.* **2023**, *35* (12), No. 2205714.

(3) Pandey, M.; Pandey, C.; Ahuja, R.; Kumar, R. Straining techniques for strain engineering of 2D materials towards flexible straintronic applications. *Nano Energy* **2023**, *109*, No. 108278.

(4) Feng, J.; Qian, X.; Huang, C.-W.; Li, J. Strain-engineered artificial atom as a broad-spectrum solar energy funnel. *Nat. Photonics* **2012**, *6* (12), 866−872.

(5) Castellanos-Gomez, A.; Roldán, R.; Cappelluti, E.; Buscema, M.; Guinea, F.; Van Der Zant, H. S.; Steele, G. A. Local strain engineering in atomically thin MoS2. *Nano Lett.* **2013**, *13* (11), 5361−5366.

(6) San-Jose, P.; Parente, V.; Guinea, F.; Roldán, R.; Prada, E. Inverse funnel effect of excitons in strained black phosphorus. *Phys. Rev. X* **2016**, *6* (3), No. 031046.

(7) Dirnberger, F.; Ziegler, J. D.; Faria Junior, P. E.; Bushati, R.; Taniguchi, T.; Watanabe, K.; Fabian, J.; Bougeard, D.; Chernikov, A.; Menon, V. M. Quasi-1D exciton channels in strain-engineered 2D materials. *Sci. Adv.* **2021**, *7* (44), No. eabj3066.

(8) Wang, J.; He, L.; Zhang, Y.; Nong, H.; Li, S.; Wu, Q.; Tan, J.; Liu, B. Locally strained 2D materials: Preparation, properties, and applications. *Adv. Mater.* **2024**, *36*, No. 2314145.

(9) Blundo, E.; Cappelluti, E.; Felici, M.; Pettinari, G.; Polimeni, A. Strain-tuning of the electronic, optical, and vibrational properties of two-dimensional crystals. *Appl. Phys. Rev.* **2021**, *8* (2), No. 021318, DOI: 10.1063/5.0037852.

(10) Lee, F.; Tripathi, M.; Salas, R. S.; Ogilvie, S. P.; Graf, A. A.; Jurewicz, I.; Dalton, A. B. Localised strain and doping of 2D materials. *Nanoscale* **2023**, *15* (16), 7227−7248.

(11) Peng, Z.; Chen, X.; Fan, Y.; Srolovitz, D. J.; Lei, D. Strain engineering of 2D semiconductors and graphene: from strain fields to band-structure tuning and photonic applications. *Light: Sci. Appl.* **2020**, *9* (1), 190.

(12) Ai, R.; Cui, X.; Li, Y.; Zhuo, X. Local Strain Engineering of Two-Dimensional Transition Metal Dichalcogenides Towards Quantum Emitters. *Nano−Micro Lett.* **2025**, *17* (1), 104.

(13) Lyu, B.; Li, H.; Jiang, L.; Shan, W.; Hu, C.; Deng, A.; Ying, Z.; Wang, L.; Zhang, Y.; Bechtel, H. A.; et al. Phonon polariton-assisted infrared nanoimaging of local strain in hexagonal boron nitride. *Nano Lett.* **2019**, *19* (3), 1982−1989.

(14) Bertolazzi, S.; Brivio, J.; Kis, A. Stretching and breaking of ultrathin MoS2. *ACS Nano* **2011**, *5* (12), 9703−9709.

(15) Park, K.-D.; Khatib, O.; Kravtsov, V.; Clark, G.; Xu, X.; Raschke, M. B. Hybrid tip-enhanced nanospectroscopy and nanoimaging of monolayer WSe2 with local strain control. *Nano Lett.* **2016**, *16* (4), 2621−2627.

(16) Xu, X.; Liang, T.; Kong, D.; Wang, B.; Zhi, L. Strain engineering of two-dimensional materials for advanced electrocatalysts. *Mater. Today Nano* **2021**, *14*, No. 100111.

(17) Hu, Y.; Zhang, F.; Titze, M.; Deng, B.; Li, H.; Cheng, G. J. Straining effects in MoS 2 monolayer on nanostructured substrates: temperature-dependent photoluminescence and exciton dynamics. *Nanoscale* **2018**, *10* (12), 5717−5724.

(18) Jasiński, J.; Balgarkashi, A.; Piazza, V.; Dede, D.; Surrente, A.; Baranowski, M.; Maude, D. K.; Banerjee, M.; Frisenda, R.; Castellanos-Gomez, A.; et al. Strain induced lifting of the charged exciton degeneracy in monolayer MoS2 on a GaAs nanomembrane. *2D Mater.* **2022**, *9* (4), No. 045006.

(19) Khestanova, E.; Guinea, F.; Fumagalli, L.; Geim, A.; Grigorieva, I. Universal shape and pressure inside bubbles appearing in van der Waals heterostructures. *Nat. Commun.* **2016**, *7* (1), No. 12587.

(20) Blundo, E.; Felici, M.; Yildirim, T.; Pettinari, G.; Tedeschi, D.; Miriametro, A.; Liu, B.; Ma, W.; Lu, Y.; Polimeni, A. Evidence of the direct-to-indirect band gap transition in strained two-dimensional WS 2, MoS 2, and WSe 2. *Phys. Rev. Res.* **2020**, *2* (1), No. 012024.

(21) Dhakal, K. P.; Roy, S.; Jang, H.; Chen, X.; Yun, W. S.; Kim, H.; Lee, J.; Kim, J.; Ahn, J.-H. Local strain induced band gap modulation and photoluminescence enhancement of multilayer transition metal dichalcogenides. *Chem. Mater.* **2017**, *29* (12), 5124−5133.

(22) Harats, M. G.; Kirchhof, J. N.; Qiao, M.; Greben, K.; Bolotin, K. I. Dynamics and efficient conversion of excitons to trions in non-uniformly strained monolayer WS2. *Nat. Photonics* **2020**, *14* (5), 324−329.

(23) Zhang, R.; Lai, Y.; Chen, W.; Teng, C.; Sun, Y.; Yang, L.; Wang, J.; Liu, B.; Cheng, H.-M. Carrier trapping in wrinkled 2D monolayer MoS2 for ultrathin memory. *ACS Nano* **2022**, *16* (4), 6309−6316.

(24) Esposito, F.; Bosi, M.; Attolini, G.; Golovynskyi, S.; Seravalli, L. Two-dimensional MoS2 for photonic applications. *Semicond. Phys., Quantum Electron. Optoelectron.* **2025**, *28* (1), 037−046.

(25) Stafford, C. M.; Harrison, C.; Beers, K. L.; Karim, A.; Amis, E. J.; VanLandingham, M. R.; Kim, H.-C.; Volksen, W.; Miller, R. D.; Simonyi, E. E. A buckling-based metrology for measuring the elastic moduli of polymeric thin films. *Nat. Mater.* **2004**, *3* (8), 545−550.

(26) Brennan, C. J.; Nguyen, J.; Yu, E. T.; Lu, N. Interface adhesion between 2D materials and elastomers measured by buckle delaminations. *Adv. Mater. Interfaces* **2015**, *2* (16), No. 1500176.

(27) Iguiñiz, N.; Frisenda, R.; Bratschitsch, R.; Castellanos-Gomez, A. Revisiting the buckling metrology method to determine the Young's modulus of 2D materials. *Adv. Mater.* **2019**, *31* (10), No. 1807150.

(28) Feldman, J. Elastic constants of 2H-MoS2 and 2H-NbSe2 extracted from measured dispersion curves and linear compressibilities. *J. Phys. Chem. Solids* **1976**, *37* (12), 1141−1144.

(29) Martella, C.; Massetti, C.; Dhungana, D. S.; Bonera, E.; Grazianetti, C.; Molle, A. Bendable silicene membranes. *Adv. Mater.* **2023**, *35* (49), No. 2211419.

(30) Li, S.-L.; Miyazaki, H.; Song, H.; Kuramochi, H.; Nakaharai, S.; Tsukagoshi, K. Quantitative Raman spectrum and reliable thickness identification for atomic layers on insulating substrates. *ACS Nano* **2012**, *6* (8), 7381−7388.

(31) Li, H.; Zhang, Q.; Yap, C. C. R.; Tay, B. K.; Edwin, T. H. T.; Olivier, A.; Baillargeat, D. From bulk to monolayer MoS2: evolution of Raman scattering. *Adv. Funct. Mater.* **2012**, *22* (7), 1385−1390.

(32) Chakraborty, B.; Matte, H. R.; Sood, A.; Rao, C. Layer-dependent resonant Raman scattering of a few layer MoS2. *J. Raman Spectrosc.* **2013**, *44* (1), 92−96.

(33) Lee, C.; Yan, H.; Brus, L. E.; Heinz, T. F.; Hone, J.; Ryu, S. Anomalous lattice vibrations of single-and few-layer MoS2. *ACS Nano* **2010**, *4* (5), 2695−2700.

(34) Tonndorf, P.; Schmidt, R.; Böttger, P.; Zhang, X.; Börner, J.; Liebig, A.; Albrecht, M.; Kloc, C.; Gordan, O.; Zahn, D. R.; et al. Photoluminescence emission and Raman response of monolayer MoS2, MoSe2, and WSe2. *Opt. Express* **2013**, *21* (4), 4908−4916.

(35) Frisenda, R.; Niu, Y.; Gant, P.; Molina-Mendoza, A. J.; Schmidt, R.; Bratschitsch, R.; Liu, J.; Fu, L.; Dumcenco, D.; Kis, A.; Lara, D. P.; Castellanos-Gomez, A. Micro-reflectance and transmittance spectroscopy: a versatile and powerful tool to characterize 2D materials. *J. Phys. D: Appl. Phys.* **2017**, *50* (7), No. 074002.

(36) Michail, A.; Delikoukos, N.; Parthenios, J.; Galiotis, C.; Papagelis, K. Optical detection of strain and doping inhomogeneities in single layer MoS2. *Appl. Phys. Lett.* **2016**, *108* (17), No. 173102, DOI: 10.1063/1.4948357.

(37) Velický, M.; Rodriguez, A.; Bousa, M.; Krayev, A. V.; Vondracek, M.; Honolka, J.; Ahmadi, M.; Donnelly, G. E.; Huang, F.; Abruna, H. D.; et al. Strain and charge doping fingerprints of the strong interaction between monolayer MoS2 and gold. *J. Phys. Chem. Lett.* **2020**, *11* (15), 6112−6118.

(38) Rodríguez, Á.; Çakıroğlu, O.; Li, H.; Carrascoso, F.; Mompean, F.; Garcia-Hernandez, M.; Munuera, C.; Castellanos-Gomez, A. Improved strain transfer efficiency in large-area two-dimensional MoS2 obtained by gold-assisted exfoliation. *J. Phys. Chem. Lett.* **2024**, *15* (24), 6355−6362.

(39) Chae, W. H.; Cain, J. D.; Hanson, E. D.; Murthy, A. A.; Dravid, V. P. Substrate-induced strain and charge doping in CVD-grown

https://doi.org/10.1021/acsanm.5c02997
ACS Appl. Nano Mater. XXXX, XXX, XXX−XXX

monolayer MoS2. *Appl. Phys. Lett.* **2017**, *111* (14), No. 143106, DOI: 10.1063/1.4998284.
(40) Feng, X.; Yu, Z. G.; Guo, H.; Li, Y.; Zhang, Y. W.; Ang, K. W. Direct Observation of Semimetal Contact Induced Charge Doping and Strain Effect in CVD-Grown Monolayer MoS2 Transistors. *Adv. Electron. Mater.* **2024**, *10* (6), No. 2300820.
(41) Kadantsev, E. S.; Hawrylak, P. Electronic structure of a single MoS2 monolayer. *Solid State Commun.* **2012**, *152* (10), 909−913.
(42) Kormányos, A.; Zólyomi, V.; Drummond, N. D.; Rakyta, P.; Burkard, G.; Fal'Ko, V. I. Monolayer MoS 2: Trigonal warping, the Γ valley, and spin-orbit coupling effects. *Phys. Rev. B* **2013**, *88* (4), No. 045416.
(43) Deng, S.; Che, S.; Debbarma, R.; Berry, V. Strain in a single wrinkle on an MoS 2 flake for in-plane realignment of band structure for enhanced photo-response. *Nanoscale* **2019**, *11* (2), 504−511.
(44) Golovynskyi, S.; Datsenko, O. I.; Dong, D.; Lin, Y.; Irfan, I.; Li, B.; Lin, D.; Qu, J. Trion binding energy variation on photo-luminescence excitation energy and power during direct to indirect bandgap crossover in monolayer and few-layer MoS2. *J. Phys. Chem. C* **2021**, *125* (32), 17806−17819.
(45) Pei, J.; Yang, J.; Xu, R.; Zeng, Y. H.; Myint, Y. W.; Zhang, S.; Zheng, J. C.; Qin, Q.; Wang, X.; Jiang, W.; Lu, Y. Exciton and trion dynamics in bilayer MoS2. *Small* **2015**, *11* (48), 6384−6390.
(46) Datsenko, O. I.; Golovynskyi, S.; Pérez-Jiménez, A. I.; Chaigneau, M.; Golovynskyi, A.; Golovynska, I.; Shevchenko, V.; Bosi, M.; Seravalli, L. Tensile strain creates trion: Excitonic photoluminescence distribution over bilayer MoS2 grown by CVD. *Physica E* **2023**, *154*, No. 115812.
(47) Wu, Q.; Nong, H.; Zheng, R.; Zhang, R.; Wang, J.; Yang, L.; Liu, B. Resolidified chalcogen precursors for high-quality 2D semiconductor growth. *Angew. Chem., Int. Ed.* **2023**, *135* (29), No. e202301501.
(48) Zhang, Y.; Wang, J.; Chen, Y.; Wu, X.; Tan, J.; Liu, J.; Nong, H.; He, L.; Wu, Q.; Zhou, G.; et al. Exclusive generation of single-atom sulfur for ultrahigh quality monolayer MoS2 growth. *J. Am. Chem. Soc.* **2024**, *146* (49), 33289−33294.
(49) Conley, H. J.; Wang, B.; Ziegler, J. I.; Haglund, R. F., Jr; Pantelides, S. T.; Bolotin, K. I. Bandgap engineering of strained monolayer and bilayer MoS2. *Nano Lett.* **2013**, *13* (8), 3626−3630.
(50) Li, Z.; Lv, Y.; Ren, L.; Li, J.; Kong, L.; Zeng, Y.; Tao, Q.; Wu, R.; Ma, H.; Zhao, B.; et al. Efficient strain modulation of 2D materials via polymer encapsulation. *Nat. Commun.* **2020**, *11* (1), No. 1151.
(51) Christopher, J. W.; Vutukuru, M.; Lloyd, D.; Bunch, J. S.; Goldberg, B. B.; Bishop, D. J.; Swan, A. K. Monolayer MoS 2 strained to 1.3% with a microelectromechanical system. *J. Microelectromech. Syst.* **2019**, *28* (2), 254−263.
(52) Çakıroğlu, O.; Island, J. O.; Xie, Y.; Frisenda, R.; Castellanos-Gomez, A. An automated system for strain engineering and straintronics of 2D materials. *Adv. Mater. Technol.* **2022**, *8*, No. 2201091.
(53) Golovynskyi, S.; Datsenko, O. I.; Perez-Jimenez, A. I.; Kuklin, A.; Chaigneau, M.; Golovynskyi, A.; Golovynska, I.; Bosi, M.; Seravalli, L. Exciton and Trion at the Perimeter and Grain Boundary of CVD-Grown Monolayer MoS2: Strain Effects Influencing Application in Nano-Optoelectronics. *ACS Appl. Nano Mater.* **2024**, *7* (13), 15570−15582.
(54) Luo, S.; Cullen, C. P.; Guo, G.; Zhong, J.; Duesberg, G. S. Investigation of growth-induced strain in monolayer MoS2 grown by chemical vapor deposition. *Appl. Surf. Sci.* **2020**, *508*, No. 145126.
(55) Rouhani, M.; Hobley, J.; Lin, K.-I.; Hofmann, M.; Yao, Y.-C.; Chang, Y.-H.; Carpick, R. W.; Schall, J. D.; Jeng, Y.-R. High-temperature strain-mediated oxidation of 2D MoS2. *Mater. Des.* **2023**, *236*, No. 112490.
(56) Carrascoso, F.; Frisenda, R.; Castellanos-Gomez, A. Biaxial versus uniaxial strain tuning of single-layer MoS2. *Nano Mater. Sci.* **2022**, *4* (1), 44−51.
(57) Avila, J.; Lorcy, S.; Dudin, P. ANTARES: Space-resolved electronic structure. *J. Electron Spectrosc. Relat. Phenom.* **2023**, *266*, No. 147362.
(58) Yun, W. S.; Han, S.; Hong, S. C.; Kim, I. G.; Lee, J. Thickness and strain effects on electronic structures of transition metal dichalcogenides: 2H-MX 2 semiconductors (M = Mo, W; X = S, Se, Te). *Phys. Rev. B* **2012**, *85* (3), No. 033305.
(59) Shi, H.; Pan, H.; Zhang, Y.-W.; Yakobson, B. I. Quasiparticle band structures and optical properties of strained monolayer MoS 2 and WS 2. *Phys. Rev. B* **2013**, *87* (15), No. 155304.

https://doi.org/10.1021/acsanm.5c02997
ACS Appl. Nano Mater. XXXX, XXX, XXX−XXX